Competing magnetic and spin-gapless semiconducting behavior in fully compensated ferrimagnetic CrVTiAl: Theory and experiment

Y. Venkateswara,[1] Sachin Gupta,[1,2] S. Shanmukharao Samatham,[1] Manoj Raama Varma,[3] Enamullah ,[4] K. G. Suresh,[1,*] and Aftab Alam[4,†]

[1]*Magnetic Materials Laboratory, Department of Physics, Indian Institute of Technology Bombay, Mumbai 400076, India*
[2]*WPI-Advanced Institute for Materials Research (WPI-AIMR), Tohoku University, Sendai 980-8577, Japan*
[3]*National Institute for Interdisciplinary Sciences and Technology (CSIR), Thiruvananthapuram, India*
[4]*Department of Physics, Indian Institute of Technology Bombay, Mumbai 400076, India*

(Received 18 July 2017; revised manuscript received 2 December 2017; published 6 February 2018)

We report the structural, magnetic, and transport properties of the polycrystalline CrVTiAl alloy along with first-principles calculations. The alloy crystallizes in a LiMgPdSn-type structure with a lattice parameter of 6.14 Å at room temperature. The absence of the (111) peak along with the presence of a weak (200) peak indicates the antisite disorder of Al with Cr and V atoms, which is different from the pure DO_3 type. Magnetization measurements reveal a magnetic transition near 710 K, a coercive field of ∼100 Oe at 3 K, and a moment of $\sim 10^{-3}\mu_B$/f.u. These observations are indicative of fully compensated ferrimagnetism in the alloy, which is confirmed by theoretical modeling. The temperature coefficient of resistivity is found to be negative, signaling the semiconducting nature. However, the absence of exponential dependence indicates the semiconducting nature with gapless/spin-gapless behavior. Electronic and magnetic properties of CrVTiAl for all three possible crystallographic configurations are studied theoretically. All the configurations are found to be different forms of semiconductors. The ground-state configuration is a fully compensated ferrimagnet with band gaps of 0.58 and 0.30 eV for the spin-up and -down bands, respectively. The next-higher-energy configuration is also fully compensated ferrimagnetic but has a spin-gapless semiconducting nature. The highest-energy configuration corresponds to a nonmagnetic, gapless semiconductor. The energy differences among these configurations are quite small (<1 mRy/atom), which hints that, at finite temperatures, the alloy exists in a disordered phase, which is a mixture of the three configurations. By taking into account the theoretical and experimental findings, we conclude that CrVTiAl is a fully compensated ferrimagnet with a predominantly spin-gapless semiconducting nature.

DOI: 10.1103/PhysRevB.97.054407

I. INTRODUCTION

Spintronics is an emerging branch of electronics in which the spin degree of freedom is added to the charge degree of electrons to realize many advantages such as nonvolatility, high processing speed, low power consumption, high storage density, etc., over conventional electronics [1–7]. The utilization of the spin degree of freedom i.e., in spintronic devices, can be found in spin diodes used in magnetic hard disks, read heads, magnetoresistive random access memory, spin transistors, tunnel diodes, vortex oscillators, etc. [8–12]. To realize spintronic devices, special materials are required; for example, their electrical conduction should be restricted to only one type of spin carrier. Such a phenomenon is seen in half-metallic ferromagnets (HMFs), spin-gapless semiconductors (SGSs), semiconducting spin filters, etc. [3,13–16]. Among the discovered materials, fully compensated ferrimagnetic (FCF) materials have gained a lot of interest recently [17–19]. Leuken and de Groot have theoretically shown that this new class of materials can show 100% spin polarization without having a net magnetic moment and gave it the name half-metallic antiferromagnets (AFMs), which was later renamed half-metallic fully compensated ferrimagnets [20–22]. However, for the antiferromagnets, symmetry demands identical densities of states (DOSs) for spin-up and spin-down bands [19,23]. Due to symmetric bands and DOS, both the spin channels equally contribute to electrical conductivity, which results in zero net spin-polarized current. On the other hand, such a scenario is not true for FCF materials, which usually contain three or more magnetic ions with moments aligned in such a way that the net magnetization is nearly zero. AFM materials contain an even number of magnetic ions in order to have inversion symmetry, whereas FCF materials must contain three or more magnetic ions to break the inversion symmetry. In certain materials, the magnetic ions are identical, while in others the ions are different. For example, in Mn_3Al, two Mn ions occupy the tetrahedral sites with a moment of $1.40\mu_B$ each (aligned in the same direction), while the other Mn occupies the octahedral site and possesses a moment of $-2.79\mu_B$. This results in a fully compensated ferrimagnetic system [24]. Its crystal structure possesses inversion symmetry, whereas the magnetic structure does not. Breaking the inversion symmetry in magnetic structure is a requirement for spintronic materials (ferromagnetic, ferrimagnetic, and fully compensated ferrimagnetic). Thus, fully compensated ferrimagnets are a special case of ferrimagnets, and they should not be confused

*suresh@phy.iitb.ac.in
†aftab@iitb.ac.in

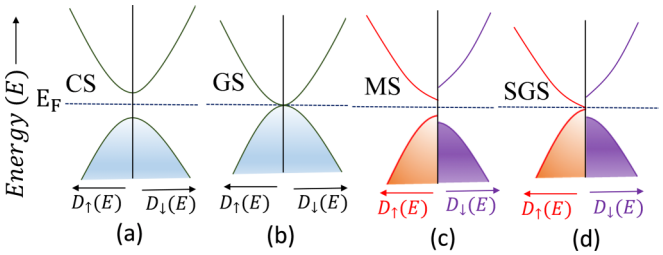

FIG. 1. Schematic density of states of various types of semiconductors. (a) Conventional semiconductor (CS) in which both spin-up (↑) and -down (↓) bands have finite and equal band gaps. (b) A gapless semiconductor (GS) where both the spin bands have a vanishing band gap. (c) A magnetic semiconductor (MS) in which the band gaps of spin-up and -down bands are finite but unequal. (d) A spin-gapless semiconductor in which any one band (up or down) is gapless while the other has a finite gap.

with antiferromagnets, which must possess magnetic inversion symmetry. Some of the unique properties and advantages of FCF materials are (i) the nearly zero magnetic moment, which creates no external stray fields, resulting in low energy losses, (ii) spin sensitivity without stray magnetic fields, which allows them not to disturb the spin character and makes them ideal for spin-polarized scanning tunneling microscope tips and improved density of circuit integration in a chip [25], (iii) the low shape anisotropy, which helps in applications in spin injection, etc. These properties make them superior to HMF materials and are very much in demand today.

Although Heusler alloys have been known for many decades, they have gained renewed interest because of the developments in the field of spintronics [4,26–30]. Özdoğan *et al.* studied the electronic and magnetic properties of quaternary Heusler alloys (QHAs) theoretically by using the full-potential nonorthogonal local-orbital minimum-basis band structure scheme [31]. Among the studied alloys, CrVTiAl has attracted a lot of interest, and preliminary band structure studies indicated it is an antiferromagnetic semiconductor [31]. Later, it was called a fully compensated ferrimagnet with distinct magnetic moments at the Cr, V, and Ti ions [21,22]. To make it clear, although a few authors have used the term AFM and others have used FCF, they essentially arrived at the same result, and as such, this is just a difference in terminology. The difference lies in the symmetry; that is, AFMs possess inversion symmetry with an even number of magnetic ions, while FCF lacks inversion symmetry and contains more than two magnetic ions, as in the case of CrVTiAl.

The schematic densities of states of different classes of semiconductors are displayed in Fig. 1. Figure 1(a) is a conventional semiconductor (CS) in which both spin-up and spin-down bands have equal band gap ΔE_g. In thermal equilibrium, the intrinsic charge carrier concentration is given by [32]

$$n_i = 2\left(\frac{k_B T}{2\pi\hbar^2}\right)^{3/2} (m_e m_h)^{3/4} e^{-(\Delta E_g/2k_B T)}. \quad (1)$$

Here m_e (m_h) is the effective mass of an electron (hole). The conductivity in CS is dominated by the exponential term. Figure 1(b) is a special case in which the gap closes ($\Delta E_g \approx 0$; for example, HgTe), in which n_i varies as $T^{3/2}$ [33]. Figure 1(c) shows a conventional magnetic semiconductor in which band gap for each spin band is finite but not equal, resulting in spin-polarized intrinsic carriers and hence its use in spin filters. Figure 1(d) is a special class of magnetic semiconductors in which one of the spin bands encounters zero gap ($\Delta E_{g\uparrow} \approx 0$) while the other has a finite gap [14,15,34]. In this case, the concentration of intrinsic spin-up carriers $n_\uparrow$, which varies as $T^{3/2}$, dominates in comparison to that of spin-down carries $n_\downarrow$, which varies in an exponential manner, and as a result, the temperature dependence of the total concentration of intrinsic carriers slightly deviates from purely $T^{3/2}$ at not too high temperatures.

An experimental investigation carried out by Stephen *et al.* has shown CrVTiAl to be a magnetic semiconductor [35], but they attributed the resistivity behavior to a combination of metallic and semiconducting contributions. According to them, the magnetization depends linearly on the field, unlike in our case. As is evident in the following sections, our experimental results for the same alloy show some striking differences. With the aim of shedding more light on the anomalous properties exhibited by this alloy, we have carried out a joint theoretical and experimental study, which reveals certain hitherto unknown aspects of the structure-property correlations of this alloy.

II. EXPERIMENTAL AND THEORETICAL DETAILS

The polycrystalline CrVTiAl alloy was prepared by arc melting the stoichiometric proportions of constituent elements with a purity of at least 99.99%. Room-temperature x-ray diffraction (XRD) patterns were collected using an X'Pert Pro diffractometer using Cu Kα radiation. The crystal structure was analyzed by Rietveld refinement using the FULLPROF suite [36].

The crystal structure of QHAs of the type $XX'YZ$ (where X, X', and Y are transition elements, and Z is the main group element) can be described by three distinct (symmetrywise inequivalent) possible arrangements of atoms [4,37]. The structure consists of four Wyckoff sites, 4a, 4b, 4c, and 4d. By fixing Z at the 4a site, the distinct configurations are (I) X at 4b, X' at 4c, and Y at the 4d site, (II) X at 4c, X' at 4b, and Y at the 4d site, and (III) X at 4d, X' at 4c, and Y at the 4b site. The structure factor for the first configuration is given by

$$F_{hkl} = 4(f_z + f_y e^{\pi i(h+k+l)} + f_x e^{\frac{\pi i}{2}(h+k+l)} + f_{x'} e^{-\frac{\pi i}{2}(h+k+l)}) \quad (2)$$

with unmixed (hkl) values. Here f_z, f_y, f_x, and $f_{x'}$ are the atomic scattering factors for atoms Z, Y, X, and X', respectively. Therefore, the magnitudes of

$$F_{111} = 4[(f_z - f_y) - i(f_x - f_{x'})], \quad (3)$$

$$F_{200} = 4[(f_z + f_y) - (f_x + f_{x'})], \quad (4)$$

$$F_{220} = 4[f_z + f_y + f_x + f_{x'}] \quad (5)$$

are used to classify the order of the crystal structure.

Magnetization measurements (2–400 K) were performed using a field-cooled warming protocol at 500 Oe using a vibrating sample magnetometer (Quantum Design).

High-temperature magnetization measurement was carried out using a superconducting quantum interference device magnetometer (magnetic property measurement system, Quantum Design). Resistivity ρ measurements were carried out using a physical property measurement system (PPMS; Quantum Design) using the four probe method, applying a 5 mA current. In order to understand the type of charge carriers and the variation of their density with temperature, we performed Hall measurement using the PPMS with a five-probe method by applying 1 A of current. Isothermal variation of Hall resistivity with field was measured at several temperatures, and its slope was used to estimate the concentration of charge carriers at those temperatures.

Theoretical details

Spin-resolved density functional theory as implemented in the QUANTUM ESPRESSO (QE) package [38] was used to calculate the band structure and magnetic properties of CrVTiAl. The exchange-correlation functional was taken within the generalized gradient approximation (GGA) in the parametrization of Perdew, Burke, and Ernzerhof (PBE) [39]. The pseudopotentials in the projector augmented-wave method [40] were generated using PSLIBRARY and QE. Self-consistent calculations were carried out using a $24 \times 24 \times 24$ k-point mesh with Methfessel-Paxton smearing with a width of 0.005 Ry, resulting in 413 k points in the irreducible wedge of the Brillouin zone. The energy convergence criterion was set to 10^{-9} Ry. The kinetic energy of the plane-wave expansion (energy cut-off E_{cut}) was restricted to 60 Ry, and charge density expansion was restricted to 700 Ry. Non-self-consistent field calculations were carried out using a $48 \times 48 \times 48$ k-point grid. The projected density of states was extracted with an smearing width of 0.0025 Ry.

The thermal charge carrier concentration was calculated using the theoretical DOS $D(E)$. The electron density above the Fermi energy E_{F} at finite temperature T is $D(E)f(E)$. Hence, the total number of thermally created electrons is

$$n_e(T) = \int_{E=0}^{\infty} D(E)f(E)dE. \tag{6}$$

Here E_F is taken as the reference level, and $f(E) = 1/[1 + \exp(-E/k_{\text{B}}T)]$ is the Fermi function. In a similar manner, the total number of thermally created holes can be found using the expression

$$n_h(T) = \int_{E=-\infty}^{0} D(E)[1 - f(E)]dE. \tag{7}$$

In an intrinsic semiconductor, at thermal equilibrium, the number of thermal electrons is equal to the number of created holes i.e., $n_{ei} = n_{hi} = \sqrt{n_e n_h}$. In addition to the thermally created charge carriers, there exists a finite number of charge carriers n_{e0} even at $T = 0$. So the total number of intrinsic carriers at a given T is $n = 2\sqrt{n_e n_h} + n_{e0}$. To obtain the number of total spin-resolved carriers, one has to replace $D(E)$ with the spin-resolved density of states. The intrinsic spin polarization is obtained with the following expression:

$$P(T) = \frac{n_\uparrow(T) - n_\downarrow(T)}{n_\uparrow(T) + n_\downarrow(T)} \times 100. \tag{8}$$

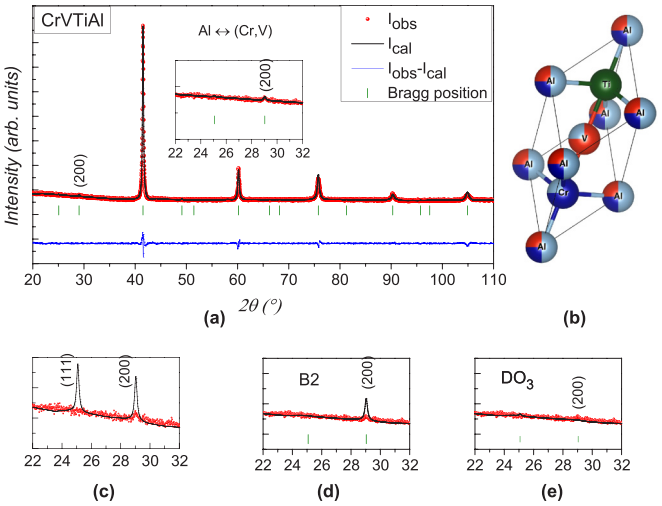

FIG. 2. (a) Rietveld refined room-temperature XRD pattern of CrVTiAl along with the best fit obtained for configuration II with antisite disorder of Al with Cr and V. The inset shows the fit near the (200) peak. (b) The corresponding crystal structure for the best fit. (c), (d), and (e) The expanded region of XRD fit near the (200) peak with no disorder, B2 disorder, and pure DO_3 disorder, respectively, for configuration II.

III. EXPERIMENTAL RESULTS

A. Crystal structure

CrVTiAl is found to crystallize in the LiMgPdSn (space group $F\bar{4}3m$, No. 216) prototype structure (or Y structure) with a lattice parameter of $a_{\text{exp}} = 6.14$ Å. Figure 2(a) shows the XRD pattern along with Rietveld refinement. The inset shows a zoomed-in region near the (200) peak. The absence of the (111) superlattice peak and the presence of the (200) superlattice peak usually indicate the existence of B2-type disorder. For this type of antisite disorder to occur, there should be a simultaneous disorder between two pairs of atoms occupying the octahedral sites and the tetrahedral sites, i.e., disorder between one pair of X and X' and another pair of Y and Z. Because of this, the resulting structure resembles the CsCl-type structure. However, the Rietveld refinement with B2 disorder did not fit well for the (200) peak for any of the three configurations mentioned earlier. As a representative case, the fit for configuration II is shown in Fig. 2(d). The observed peak intensity was much less than the calculated value for this peak. Subsequently, it was fitted to a DO_3-type antisite disorder (for the three configurations), which underestimated the intensity of the (200) peak. Figure 2(e) shows the fit for configuration II with DO_3 disorder. The best fit was obtained by considering an antisite disorder (25% each) of Al at Cr and V sites for configuration II [see the main panel of Fig. 2(a); its structure is in Fig. 2(b)]. This is due to the fact that Cr, V, and Al have nearly the same electronegativity values. Therefore, our detailed Rietveld refinement clearly shows that the alloy crystallizes in configuration II with antisite disorder of Al with Cr and V. It may be noted that the disorder is neither B2 nor purely DO_3.

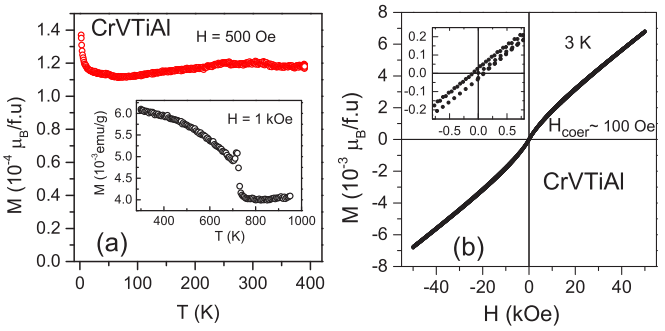

FIG. 3. (a) Temperature dependence of magnetization of CrVTiAl. The inset shows the data in the high-temperature regime. (b) Field dependence of magnetization at 3 K. The inset shows the magnetization on a zoomed-in scale.

B. Magnetic and transport properties

For QHAs composed of at least two elements with less than a half-filled number of d electrons, the saturation magnetization obeys the Slater-Pauling (SP) rule [31,41,42],

$$M = (N - 18)\mu_B/\text{f.u.}, \tag{9}$$

where N is the total number of valence electrons in the alloy.

Figures 3(a) and 3(b) show the M-T and M-H data, which clearly indicate a very small moment on CrVTiAl ($\sim 10^{-3}\mu_B$/f.u.) and a high magnetic ordering temperature [$\sim$710 K; see the inset of Fig. 3(a)]. The M-H curve, as shown in Fig. 3(b), has a low, but nonzero, hysteresis (see also the inset). The observation of hysteresis is in contrast to the data reported by Stephen *et al.* [35]. The linear part is found to be in agreement with that reported by Stephen *et al.*, while the ferromagneticlike component shows a saturation value of $1.0 \times 10^{-3}\mu_B$/f.u. The nonzero hysteresis may be due to the different temperature dependencies of the three sublattices (Cr, V, and Ti), giving rise to a ferromagneticlike behavior in our completely phase pure sample. However, at this point it is not possible to rule out some contribution from any small deviation from the 1:1:1:1 stoichiometry. We would also like to mention that such low, but finite, hysteresis is not uncommon in FCF alloys, as has been reported in $Mn_{1.5}FeV_{0.5}Al$ [18] and MnCrVAl [43], which are known to be FCF. Furthermore, the outcome of nearly zero moment is consistent with the SP rule, which is a prerequisite for spintronics materials. Therefore, results of M-T and M-H measurements prompt us to believe that CrVTiAl is a fully compensated ferrimagnet and not a simple antiferromagnet, as also revealed by our theoretical results.

Figure 4(a) shows the temperature dependence of the electrical resistivity of CrVTiAl in a few representative magnetic fields. A cursory look at the data suggests a semiconducting behavior with a negative temperature coefficient ($d\rho/dT < 0$). There is no regime of temperature in which the sample shows the metallic behavior, unlike in the report by Stephen *et al.* [35]. It is also found that the dependence of resistivity on field is almost negligible. The larger resistivity seen in our sample compared to that of Stephen *et al.* is in agreement with the prediction of a purely semiconducting nature (as per our theoretical calculations). Generally, for intrinsic semiconductors, the carrier concentration $n(T)$ is dominantly described by exponential dependence, as given in Eq. (1). The absence of such a term in CrVTiAl along with the quasilinear temperature dependence indicates two possibilities: simple gapless or spin-gapless semiconducting behavior.

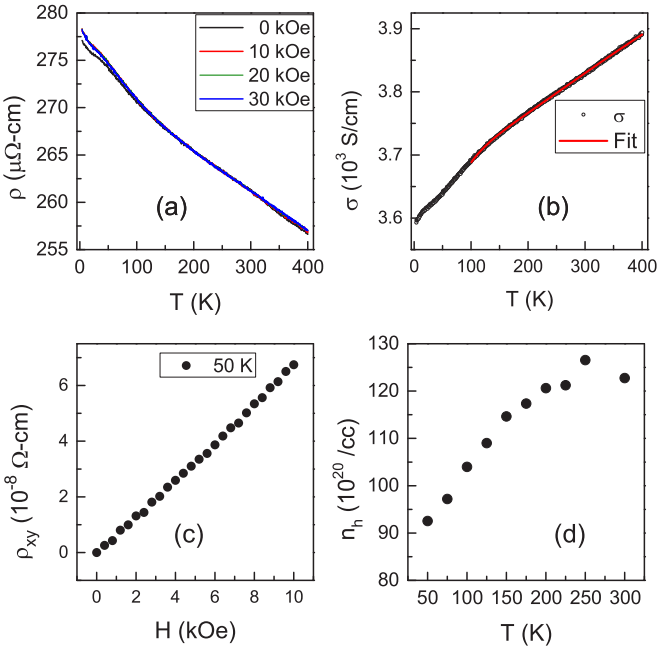

FIG. 4. (a) Temperature dependence of electrical resistivity in different fields for CrVTiAl. (b) Variation of electrical conductivity with temperature in zero field along with the fit (above 100 K) using Eq. (10). (c) Hall resistivity as a function of field at 50 K. (d) Temperature dependence of hole-carrier concentration.

Two-carrier model. In order to further understand the gapless behavior and the type of charge carriers, we have adopted a two-carrier model [24,32] according to which the conductivity σ can be modeled as the sum of electronic and hole contributions as follows:

$$\sigma(T) = \sigma_e + \sigma_h = en_e\mu_e + en_h\mu_h, \tag{10}$$

where e and h refer to the electronic and hole components, respectively. Here $n_e \sim n_{e0}\exp(-\Delta E_e/k_BT)$, and $n_h \sim n_{h0}\exp(-\Delta E_h/k_BT)$. ΔE are the gaps for the two carriers. The mobilities are given by $\mu_i = (a_iT + b_i)^{-1} = \mu_{i0}/(a_i'T + 1)$, where each carrier (electron or hole) channel i has different values of a and b. The term involving a results from electron-phonon scattering, while those involving b correspond to the mobility due to defects at $T = 0$ K. Incorporating these expressions, the final equation (10) can be expressed as

$$\sigma(T) = A_e(T)e^{-(\Delta E_e/k_BT)} + A_h(T)e^{-(\Delta E_h/k_BT)}. \tag{11}$$

Here, $A_i(T) = en_{i0}\mu_{i0}/(1 + a_i'T)$ for $i = e$ and h. The above equation is fitted to the conductivity data from 100 to 400 K, as shown by the red curve in Fig. 4(b) for zero field. Fitting to this model gives temperature coefficients a_e' and a_h' that are negligibly small (close to zero), suggesting that the mobility of CrVTiAl is significantly dominated by defect scattering rather than phonons. The estimated gaps are $\Delta E_e \sim 63.4$ meV and $\Delta E_h \sim 0.3$ meV. Because the coefficients a_i are negligibly

TABLE I. Relaxed lattice parameter a_0, atom-projected magnetic moments, total moments μ_B, and total energy E_0 for configurations I, II, and III of CrVTiAl.

Type	a_0 (Å)	m^{Cr}	m^{V}	m^{Ti}	m^{Total}	E_0 (Ry/atom)
I	6.08	0.00	0.00	0.00	0.00	− 171.370934
II	6.15	2.25	− 1.26	− 0.98	0.00	− 171.370997
III	6.19	2.80	− 2.29	− 0.49	0.00	− 171.371658

small, $A_e(T)$ and $A_h(T)$ can be considered to be almost T independent, and their fitted values are $A_e \sim 696$ S/cm and $A_h \sim 3810$ S/cm. It is observed from Fig. 4(c) that the Hall coefficient carries positive sign, indicating that the majority carriers are holes. Thus, the estimated low-gap term associated with the holes [in Eq. (11)] is justified. The lower bound on the ratio (σ_h/σ_e) at elevated temperatures ($k_B T \gg \Delta E_e$) is ~5. At $T = 300$ K, $\sigma_h \approx 3770$ S/cm, while $\sigma_e \approx 60$ S/cm; that is, the hole contribution to the conductivity is nearly 60 times the electron contribution.

We have also measured the Hall resistivity ρ_{xy} as a function of field at a few representative temperatures. Figure 4(c) shows $\rho_{xy}(H)$ at 50 K. The hole-carrier concentration is found by neglecting the electron contribution in the following equation [44]:

$$R_H = \frac{\mu_h^2 n_h - \mu_e^2 n_e}{e(\mu_h n_h + \mu_e n_e)^2}, \tag{12}$$

which reduces to $1/(n_h e)$. The estimated carrier concentration is plotted as a function of temperature in Fig. 4(d). The carrier concentration is in the range of $10^{22}/\text{cm}^3$, which is an order higher than our calculated value. The difference may be partly attributed to the neglect of the electron contribution. Additionally, the presence of disorder can, of course, play an important role in creating additional states around the Fermi level, contributing carriers to the conduction. The calculated mobility of holes is found to be ~2.2 $\text{cm}^2/\text{V s}$, which is typically low for semiconducting materials, and this supports the presence of impurity states at the Fermi level arising due to disorder.

IV. THEORETICAL RESULTS

We have fully relaxed the experimentally formed crystal structure (space group 216) in three distinct configurations, I, II, and III, as described in Sec. II. The whole idea of performing these simulations was to get a better understanding of the XRD results [e.g., the absence of the (111) peak], which is not enough to clarify a few of the structural aspects. Table I shows the relaxed lattice parameter a_0, total and atom-projected magnetic moments, and the total energy E_0 for the three configurations.

Among these, configuration III was found to be energetically the most stable one, with lattice parameter $a_0 = 6.19$ Å. The total energy difference among the three configurations is less than 1 mRy/atom which hints that at finite temperatures, CrVTiAl could be a mixture of these three configurations, leading to the observed disorder. In order to understand the effect of this disorder, we studied all three configurations in detail.

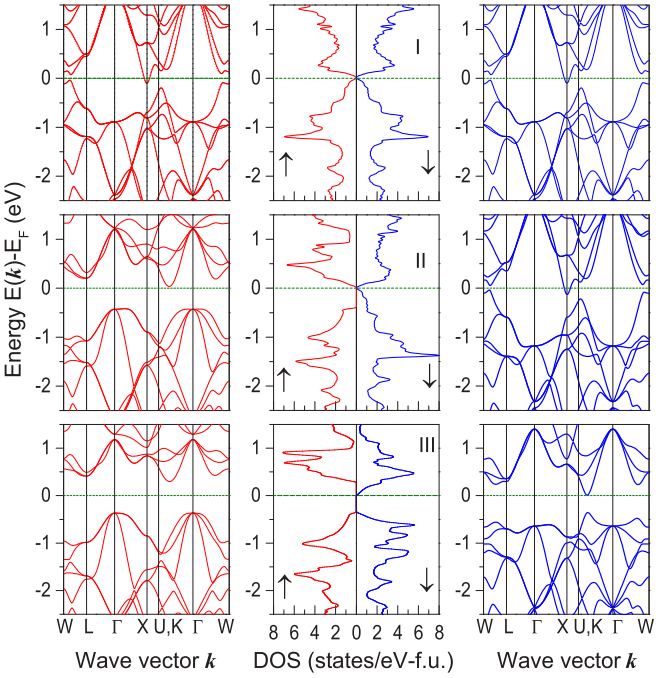

FIG. 5. Spin-polarized band structure and DOS for configurations I, II, and III of CrVTiAl at relaxed lattice parameters a_0. Left bands correspond to spin up, while the right column shows spin down.

The calculated spin-polarized band structure and DOS for all three configurations are shown in Fig. 5. Calculations for all of them were initiated with a ferrimagnetic arrangement of spins with moments at Cr atoms aligned antiparallel to those of V and Ti. This was done keeping in mind the vanishingly small experimental net moment (see the previous section) and other theoretical reports where a ferrimagnetic arrangement was proposed to be the stable phase. In our case, configuration I converged to a nonmagnetic phase with identical spin-up and -down bands, and consequently, it has the lowest magnetic ordering temperature. Both spin-up and -down bands are gapless, with nearly zero DOS at E_F, indicating the gapless nature. It acquires an indirect band gap with a conduction band minimum touching at the X point and a valence band maximum at the other k point. Figure 6(a) shows the Fermi surface plot for configuration I. As expected, both the spin-up and -down Fermi surfaces are identical, with a tiny spherical shape, and are shared by neighboring Brillouin zones. The essential features of the DOS and band structure remain unchanged at a_{exp}, and hence, physical properties in this configuration (I) (transport and magnetic) are robust.

In the case of configuration II, irrespective of the initial magnetic moments at each site, the calculations converged in a ferrimagnetic arrangement with Cr moments aligned antiparallel to V and Ti. For this configuration, DOS and band structure for the spin-down channel mostly resemble those of configuration I, except for the shape and size of the Fermi surface at the X point, indicating the gapless nature for the spin-down channel. The shape of the Fermi surface, as shown in Fig. 6(b), is oblate, centered at the X point, and equally shared by neighboring Brillouin zones. The size of the surface is more than double that of configuration I. There is almost no change in the DOS

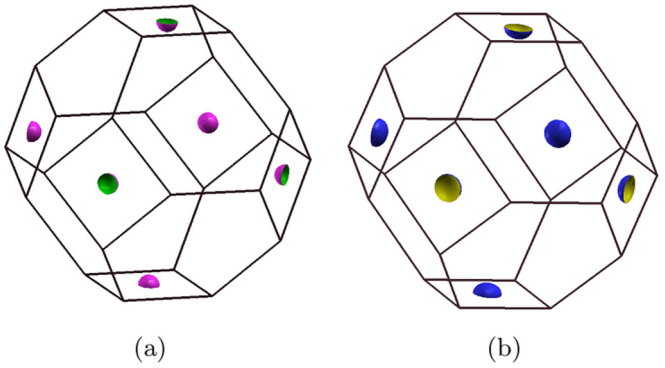

FIG. 6. (a) The Fermi surface (FS) is the same for both spin-up and -down bands of configuration I. It has a spherical shape and crosses at the X point. (b) The Fermi surface for the spin-down band of configuration II. It has an oblate shape and crosses at the X point. Configuration III does not have a FS.

and band structure of the spin-down channel with a_0 and a_{exp}, indicating that gapless nature of spin-down channel is robust against small changes in a. On the other hand, DOS and band structure for the spin-up channel show a clear indirect band gap of $\Delta E_g^{\uparrow} = 0.36$ eV, revealing a semiconducting nature. There is no observable change in $\Delta E_g^{\uparrow}$ with the lattice parameter, indicating that the semiconducting nature of the compound is also robust against small changes in a. Due to the absence of a symmetric DOS and band structure along with relatively high absolute magnetization (4.64 μ_B/f.u.), its magnetic ordering temperature is expected to be very high. Such a phase with zero gap in one spin band and finite gap in the other gives rise to a fully compensated ferrimagnetic, spin-gapless semiconductor.

Similar to configuration II, configuration III is also found to be ferrimagnetic. However, the latter has $\Delta E_g^{\uparrow} = 0.58$ eV and $\Delta E_g^{\downarrow} = 0.30$ eV at a_0, indicating that it is a magnetic semiconductor. Spin-up and -down gaps are reduced to 0.55 and 0.25 eV, respectively, at a_{exp}. The absence of Fermi surfaces (no states at E_F) for both spin channels also confirms the magnetic semiconducting nature. The presence of large exchange-splitting gaps and a large absolute magnetization (5.92μ_B/f.u.) indicates a large magnetic ordering temperature.

All the properties of configuration III (such as magnetic state, $\Delta E_g^{\uparrow,\downarrow}$. etc.), which correspond to ground-state one, are in good agreement with the earlier reports by Özdoğan *et al.*, with the exception of the sign of moments on the three ions. As a result, DOS and band structure are interchanged for spin-up and -down electrons. In addition, Özdoğan *et al.* reported a small positive moment on Al ions which also has an opposite sign in the current study. Notably, Cr and V moments are aligned in opposite directions, and the resulting moment is compensated by Ti ions (see Table I).

It is important to note that all the configurations show different forms of semiconductors, with two of them converged to the ferrimagnetic state. In order to understand the true nature of the semiconductor, it is quite important to study the temperature dependence of the transport properties, i.e., the intrinsic carrier concentration and the spin polarization P. Figure 7 shows the calculated temperature dependence of these quantities for the three configurations. Configuration I, being almost nonmagnetic, has a negligible spin polarization, although it indeed has a finite carrier concentration due to the small number of states at the Fermi level E_F. For configurations II and III, the spin-up carrier concentration is negligibly small due to the vanishing states at E_F. The spin-down carrier concentration, on the other hand, is large but has a very different nature of T dependence for the two configurations (II and III). Interestingly, in the case of configuration III, n shows an almost straight-line behavior, which is neither exponential nor $T^{3/2}$. The magnitude, however, is much smaller (by two orders of magnitude) than in the other two configurations. Spin-polarization values for these two configurations (II and III) are high.

V. DISCUSSION AND CONCLUSION

Experimental results indicate the possibility of CrVTiAl being a fully compensated ferrimagnet with antisite disorder of Al with Cr and V atoms. First-principles calculations within the GGA approximation predict configuration III is the ground state, which is a fully compensated ferrimagnet with unequal band gaps for spin-up and -down bands. However, the energy differences among the three configurations (I, II, and III) are

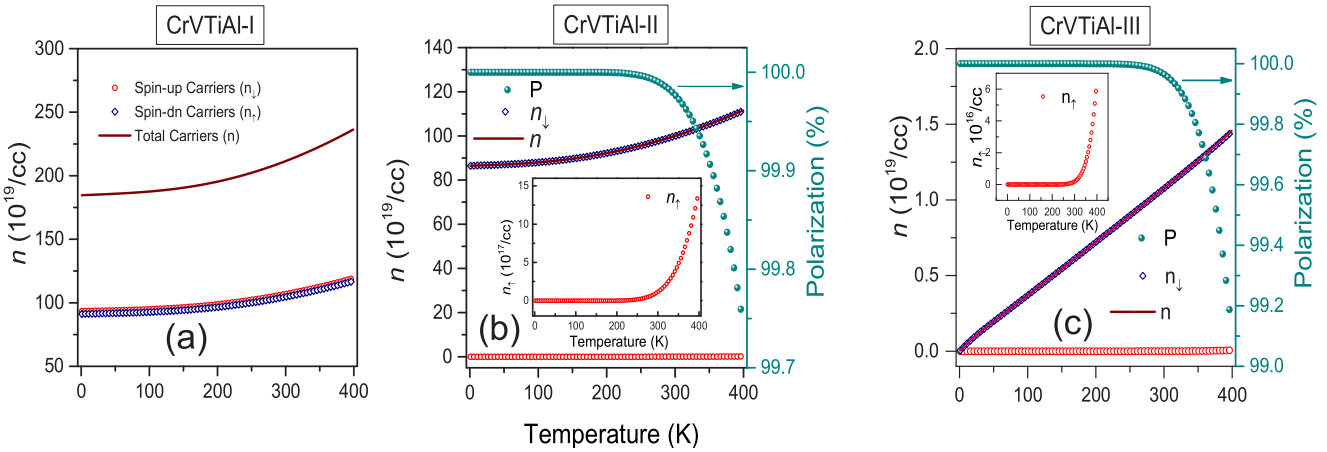

FIG. 7. Spin-resolved intrinsic carrier concentration (left axis) and spin polarization (right axis) vs temperature (3–400 K) for configurations I (left), II (middle), and III (right) of CrVTiAl.

small (<1 mRy ≈ 158 K), which indicates the possibility of a mixed phase (disordered) at finite T. One can consider the disordered state to be a linear combination of all three independent configurations (with probabilities proportional to their Boltzmann factors), yielding either a spin-gapless semiconductor, gapless semiconductor, or magnetic semiconductor with reduced band gaps. This concept originates from the fact that the disordered Kohn-Sham (KS) orbitals $\Phi_{\rm dis}$ can be written as a linear combination of KS orbitals Φ of each configuration, i.e., $\Phi_{\rm dis} = c_{\rm I}\Phi_{\rm I} + c_{\rm II}\Phi_{\rm II} + c_{\rm III}\Phi_{\rm III}$, where $c_i \propto \exp(-E_0^i/k_{\rm B}T)$. Such a linear combination is possible due to the fact that all three pure configurations have a vanishing DOS at the Fermi level, unlike most of the reported cases in which certain configurations alone have a finite number of states at $E_{\rm F}$. At the observation level, the above linear combination presents itself as having a predominantly SGS nature because the first term is energetically least attainable and nonmagnetic, while the third term is not effective as the DOS $D_{\uparrow,\downarrow}(E)$ is zero at the Fermi level ($E_g^{\uparrow,\downarrow} \gg k_{\rm B}T$). In fact, our XRD refinement indeed shows that configuration II is the most preferred one by considering antisite disorder. The above scenario can change if there are impurities, which will alter the SGS nature seen in our sample [35].

In conclusion, we identified the true crystallographic and magnetic ground states of CrVTiAl with the help of a joint theoretical and experimental investigation. While the magnetic ground state is uniquely identified as a fully compensated ferrimagnet, the balance between the spin-gapless nature and the magnetic semiconducting nature appears to be quite delicate, according to the theoretical calculations. However, by combining the experimental (x-ray diffraction, resistivity, and Hall) and theoretical results, we feel that it is reasonable to conclude that the alloy is predominantly a spin-gapless semiconductor at temperatures close to room temperature.

ACKNOWLEDGMENTS

Y.V. acknowledges the financial help provided by IIT Bombay. A.A. acknowledges DST-SERB (SB/FTP/PS-153/2013) for funding to support this research. S.S.S. and E. acknowledge Indian Institute of Technology, Bombay for the financial support through the Institute Post Doctoral Fellowship.

Y.V. and S.G. contributed equally to this work.

[1] S. A. Wolf, D. D. Awschalom, R. A. Buhrman, J. M. Daughton, S. von Molnár, M. L. Roukes, A. Y. Chtchelkanova, and D. M. Treger, Science **294**, 1488 (2001).
[2] I. Žutić, J. Fabian, and S. Das Sarma, Rev. Mod. Phys. **76**, 323 (2004).
[3] C. Felser, G. Fecher, and B. Balke, Angew. Chem., Int. Ed. **46**, 668 (2007).
[4] T. Graf, C. Felser, and S. S. Parkin, Prog. Solid State Chem. **39**, 1 (2011).
[5] G. A. Prinz, Science **282**, 1660 (1998).
[6] S. D. Sarma, Am. Sci. **89**, 516 (2001).
[7] S. D. Sarma, J. Fabian, X. Hu, and I. Zutic, IEEE Trans. Magn. **36**, 2821 (2000).
[8] A. Hirohata and K. Takanashi, J. Phys. D **47**, 193001 (2014).
[9] J. Wunderlich, B.-G. Park, A. C. Irvine, L. P. Zârbo, E. Rozkotová, P. Nemec, V. Novák, J. Sinova, and T. Jungwirth, Science **330**, 1801 (2010).
[10] D. D. Awschalom and M. E. Flatté, Nat. Phys. **3**, 153 (2007).
[11] W. Zhao and G. Prenat, *Spintronics-Based Computing* (Springer, Berlin, 2015).
[12] J.-M. Hu, Z. Li, L.-Q. Chen, and C.-W. Nan, Nat. Commun. **2**, 553 (2011).
[13] R. A. de Groot, F. M. Mueller, P. G. van Engen, and K. H. J. Buschow, Phys. Rev. Lett. **50**, 2024 (1983).
[14] X. L. Wang, Phys. Rev. Lett. **100**, 156404 (2008).
[15] S. Ouardi, G. H. Fecher, C. Felser, and J. Kübler, Phys. Rev. Lett. **110**, 100401 (2013).
[16] I. Galanakis, K. Özdoğan, and E. Şaşioğlu, AIP Adv. **6**, 055606 (2016).
[17] X. Wang, Z. Cheng, J. Wang, X.-L. Wang, and G. Liu, J. Mater. Chem. C **4**, 7176 (2016).
[18] R. Stinshoff, A. K. Nayak, G. H. Fecher, B. Balke, S. Ouardi, Y. Skourski, T. Nakamura, and C. Felser, Phys. Rev. B **95**, 060410 (2017).
[19] M. E. Jamer, B. A. Assaf, G. E. Sterbinsky, D. Arena, L. H. Lewis, A. A. Saúl, G. Radtke, and D. Heiman, Phys. Rev. B **91**, 094409 (2015).
[20] H. van Leuken and R. A. de Groot, Phys. Rev. Lett. **74**, 1171 (1995).
[21] I. Galanakis, K. Özdoğan, and E. Şaşioğlu, J. Phys. Condens. Matter **26**, 379501 (2014).
[22] K. Özdoğan, E. Şaşioğlu, and I. Galanakis, Comput. Mater. Sci. **110**, 77 (2015).
[23] M. Tas, E. Şaşioğlu, C. Friedrich, S. Blügel, and I. Galanakis, J. Appl. Phys. **121**, 053903 (2017).
[24] M. E. Jamer, Y. J. Wang, G. M. Stephen, I. J. McDonald, A. J. Grutter, G. E. Sterbinsky, D. A. Arena, J. A. Borchers, B. J. Kirby, L. H. Lewis, B. Barbiellini, A. Bansil, and D. Heiman, Phys. Rev. Appl. **7**, 064036 (2017).
[25] M. Bode, Rep. Prog. Phys. **66**, 523 (2003).
[26] C. Felser and G. Fecher, *Spintronics: From Materials to Devices* (Springer, Dordrecht, 2013).
[27] C. Y. Fong, J. E. Pask, and L. H. Yang, *Half-Metallic Materials and Their Properties*, EBSCO ebook Academic Collection (Imperial College Press, London, 2013).
[28] C. Felser and A. Hirohata, *Heusler Alloys: Properties, Growth, Applications*, Springer Series in Materials Science 222 (Springer International Publishing AG, Switzerland, 2015).
[29] K. Sato, E. Saitoh, A. Willoughby, P. Capper, and S. Kasap, *Spintronics for Next Generation Innovative Devices*, Wiley Series in Materials for Electronic and Optoelectronic Applications (Wiley, Hoboken, NJ, 2015).
[30] W. E. Pickett and J. S. Moodera, Phys. Today **54**(5), 39 (2001).
[31] K. Özdoğan, E. Şaşioğlu, and I. Galanakis, J. Appl. Phys. **113**, 193903 (2013).
[32] C. Kittel, *Introduction to Solid State Physics*, 7th ed. (Wiley India, New Delhi, 2007), p. 219.
[33] J. Tsidilkovski, *Electron Spectrum of Gapless Semiconductors*, Springer Series in Solid-State Sciences (Springer, Berlin, 2012).

[34] L. Bainsla, A. I. Mallick, M. M. Raja, A. K. Nigam, B. S. D. C. S. Varaprasad, Y. K. Takahashi, A. Alam, K. G. Suresh, and K. Hono, Phys. Rev. B **91**, 104408 (2015).
[35] G. M. Stephen, I. McDonald, B. Lejeune, L. H. Lewis, and D. Heiman, Appl. Phys. Lett. **109**, 242401 (2016).
[36] J. Rodríguez-Carvajal, Physica B (Amsterdam, Neth.) **192**, 55 (1993).
[37] Enamullah, Y. Venkateswara, S. Gupta, M. R. Varma, P. Singh, K. G. Suresh, and A. Alam, Phys. Rev. B **92**, 224413 (2015).
[38] P. Giannozzi, S. Baroni, N. Bonini, M. Calandra, R. Car, C. Cavazzoni, D. Ceresoli, G. L. Chiarotti, M. Cococcioni, I. Dabo, A. D. Corso, S. de Gironcoli, S. Fabris, G. Fratesi, R. Gebauer, U. Gerstmann, C. Gougoussis, A. Kokalj, M. Lazzeri, L. Martin-Samos, N. Marzari, F. Mauri, R. Mazzarello, S. Paolini, A. Pasquarello, L. Paulatto, C. Sbraccia, S. Scandolo, G. Sclauzero, A. P. Seitsonen, A. Smogunov, P. Umari, and R. M. Wentzcovitch, J. Phys. Condens. Matter **21**, 395502 (2009).
[39] J. P. Perdew, K. Burke, and M. Ernzerhof, Phys. Rev. Lett. **77**, 3865 (1996).
[40] G. Kresse and D. Joubert, Phys. Rev. B **59**, 1758 (1999).
[41] N. Zheng and Y. Jin, J. Magn. Magn. Mater. **324**, 3099 (2012).
[42] Q. Gao, H.-H. Xie, L. Li, G. Lei, J.-B. Deng, and X.-R. Hu, Superlattices Microstruct. **85**, 536 (2015).
[43] P. Kharel, J. Herran, P. Lukashev, Y. Jin, J. Waybright, S. Gilbert, B. Staten, P. Gray, S. Valloppilly, Y. Huh, and D. J. Sellmyer, AIP Adv. **7**, 056402 (2017).
[44] A. C. Melissinos, *Experiments in Modern Physics* (Academic Press, An Imprint of Elsevier, California, 1966), pp. 86–87.